

A Neptune-sized transiting planet closely orbiting a 5–10-million-year-old star

Trevor J. David¹, Lynne A. Hillenbrand¹, Erik A. Petigura², John M. Carpenter³, Ian J. M. Crossfield⁴, Sasha Hinkley⁵, David R. Ciardi⁶, Andrew W. Howard⁷, Howard T. Isaacson⁸, Ann Marie Cody⁹, Joshua E. Schlieder⁹, Charles A. Beichman⁶ & Scott A. Barenfeld¹

Theories of the formation and early evolution of planetary systems postulate that planets are born in circumstellar disks, and undergo radial migration during and after dissipation of the dust and gas disk from which they formed^{1,2}. The precise ages of meteorites indicate that planetesimals—the building blocks of planets—are produced within the first million years of a star’s life³. Fully formed planets are frequently detected on short orbital periods around mature stars. Some theories suggest that the *in situ* formation of planets close to their host stars is unlikely and that the existence of such planets is therefore evidence of large-scale migration^{4,5}. Other theories posit that planet assembly at small orbital separations may be common^{6–8}. Here we report a newly born, transiting planet orbiting its star with a period of 5.4 days. The planet is 50 per cent larger than Neptune, and its mass is less than 3.6 times that of Jupiter (at 99.7 per cent confidence), with a true mass likely to be similar to that of Neptune. The star is 5–10 million years old and has a tenuous dust disk extending outward from about twice the Earth–Sun separation, in addition to the fully formed planet located at less than one-twentieth of the Earth–Sun separation.

The star [PGZ2001] J161014.7–191909, hereafter K2-33, is an M-type star several million years (Myr) old that was observed by NASA’s Kepler Space Telescope during campaign 2 of the K2 mission. The star was identified as one of more than 200 candidate planet hosts in a systematic search for transits in K2 data⁹. As part of our ongoing study of the pre-main-sequence population of Upper Scorpius observed by K2, we independently verified and analysed the planetary transit signal. We acquired radial velocity and high spatial resolution observations at the W. M. Keck Observatory to confirm the detection of the planet, named K2-33 b, and to measure its size and mass.

Within the 77.5-day photometric time series of K2-33 ($Kp = 14.3$ mag), there are periodic dimmings of 0.23% lasting 4.2 h and occurring every 5.4 days (Fig. 1). The ensemble of transits are detected at a combined signal-to-noise ratio of about 32. During the K2 observations, cool, dark regions on the stellar surface (starspots) rotated in and out of view, producing semi-sinusoidal brightness variations of $\sim 3\%$ peak-to-trough amplitude with a periodicity of 6.3 ± 0.2 days (Extended Data Fig. 1). We removed the starspot variability before modelling the transit events. We fitted the transit profiles using established methods¹⁰, measuring the planet’s size relative to its host star and its orbital geometry (Table 1).

K2-33 is a member of the Upper Scorpius OB association^{11,12}, the nearest site to Earth of recent massive star formation (at a distance of 145 ± 20 pc). Approximately 20% of low-mass stars in Upper Scorpius host protoplanetary disks¹³, indicating that planet formation is ongoing in the region but in an advanced stage or completed for the majority of stars. The age of the stellar association is 5–10 Myr,

as assessed from kinematics, the Hertzsprung–Russell diagram, and eclipsing binary analyses. The youth of K2-33 itself is based on the spectroscopic indicators of enhanced hydrogen emission and lithium absorption^{11,12}, which we confirm from Keck spectra (Table 1). Furthermore, the stellar rotation rate we measure via broadening of absorption lines in the spectra and via the starspot period (Table 1), is rapid relative to field-age stars of similar mass¹⁴. We determined the star’s systemic radial velocity (Table 1) to be consistent with the mean value for Upper Scorpius members¹⁵. Previously, proper motions were used to assess the probability of membership in the association at 99.9% (ref. 16). Finally, the positions of the star in the Hertzsprung–Russell and temperature–density diagrams (Extended Data Fig. 2) are consistent with the sequence of low-mass members of Upper Scorpius¹².

The inferred planetary size and mass depend directly upon the host star size and mass. We evaluated the effective temperature and luminosity from our newly determined spectral type (Table 1), extinction-corrected catalogue near-infrared photometry, and empirical pre-main-sequence calibrations^{17,18}. With the temperature and luminosity, we derive a stellar radius from the Stefan–Boltzmann law of $R_* = (1.1 \pm 0.1)R_\odot$, where R_\odot is the radius of the Sun. The radius uncertainty is calculated accounting for recommended errors in temperature¹⁷, photometric errors, and assuming an association depth comparable to its width on the sky. Combining the stellar radius with the planet-to-star radius ratio determined from the K2 light-curve fit, we infer a planetary radius for the companion of $R_p = (5.8 \pm 0.6)R_\oplus$, where R_\oplus is Earth’s radius, or about 50% larger than Neptune.

We estimate a stellar mass of $M_* = (0.31 \pm 0.05)M_\odot$, where M_\odot is the mass of the Sun, by interpolation among pre-main-sequence stellar evolution models¹⁹, consistent with a previously reported value²⁰. The mass uncertainty assumes normal error distributions in temperature and luminosity. As there is no evidence for radial velocity variations among four high-dispersion Keck spectra (Extended Data Table 1), the planet mass is constrained from the maximum-amplitude Keplerian curve that is consistent within the errors with all radial velocity measurements (Extended Data Fig. 3). Given the transit ephemeris and assuming a circular, edge-on orbit, the expected stellar reflex velocity is a sinusoid having a single free parameter: the semi-amplitude. Radial velocity semi-amplitudes of $>900 \text{ m s}^{-1}$ are ruled out at 99.7% confidence, corresponding to a 3σ upper limit on the mass of K2-33 b of $3.6M_{\text{Jup}}$, where M_{Jup} is the mass of Jupiter.

The true mass of K2-33 b is likely to be at least an order of magnitude smaller. There are seven known exoplanets of similar size ($R_p = 4.8R_\oplus$ – $6.6R_\oplus$) with densities measured to 50% or better. These planets have masses ranging from $(6.3 \pm 0.8)M_\oplus$ (for Kepler-87 c; where M_\oplus is Earth’s mass) to $(69 \pm 11)M_\oplus$ (for CoRoT-8 b) owing to varying core masses. Thus, plausible masses of K2-33 b range from about $6M_\oplus$ to

¹Cahill Center for Astronomy and Astrophysics, California Institute of Technology, Pasadena, California 91125, USA. ²Division of Geological and Planetary Sciences, California Institute of Technology, Pasadena, California 91125, USA. ³Joint ALMA Observatory, Avenida Alonso de Córdova 3107, Vitacura, Santiago, Chile. ⁴Lunar and Planetary Laboratory, University of Arizona, Tucson, Arizona 85721, USA. ⁵Physics Department, University of Exeter, Stocker Road, Exeter EX4 4QL, UK. ⁶NASA Exoplanet Science Institute, California Institute of Technology, Pasadena, California 91125, USA. ⁷Institute for Astronomy, University of Hawai’i at Mānoa, Honolulu, Hawaii 96822, USA. ⁸Department of Astronomy, University of California, Berkeley, California 94720, USA. ⁹NASA Ames Research Center, Mountain View, California 94035, USA.

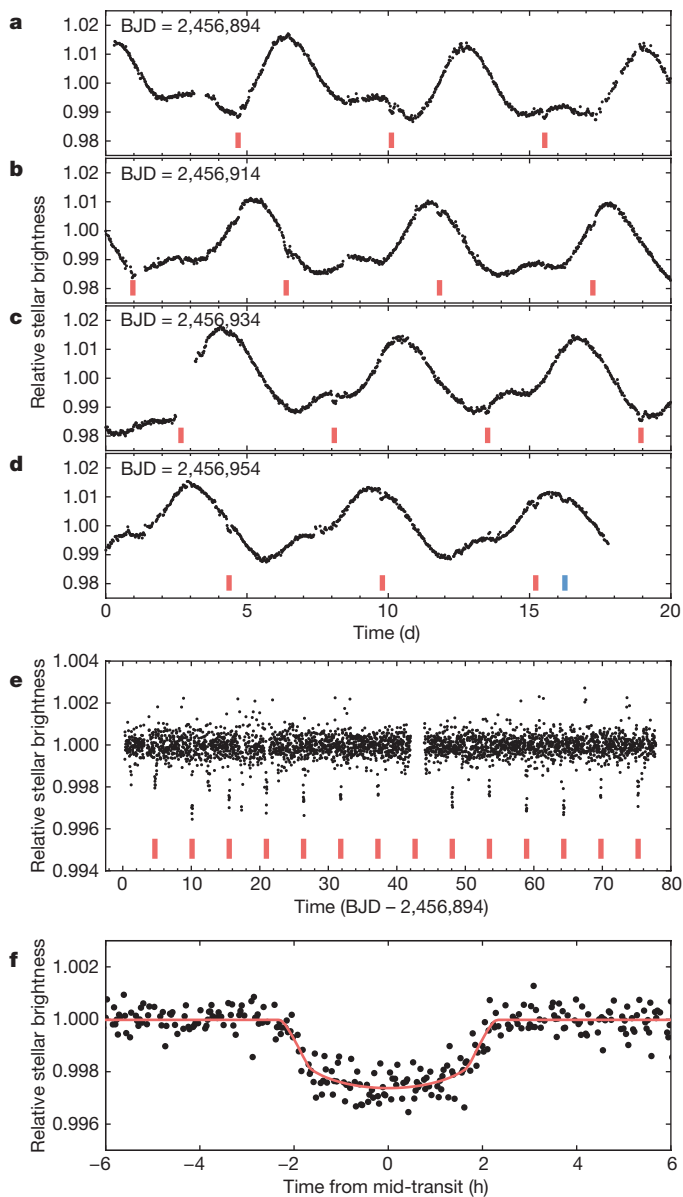


Figure 1 | Light curve of K2-33. a–d, K2 photometry in twenty-day segments. K2-33 varies in brightness by $\sim 3\%$ every 6.3 days owing to the rotation of its spotted surface. The planet K2-33 b transits its star every 5.4 days (red ticks). Another potential transit (blue tick in d), distinct from the K2-33 b transits, is possibly caused by a second planet with an orbital period of >77.5 days. e, Stellar variability was removed before fitting transits. The data gap is due to excluded observations where the variability fit inadequately captured a systematic artefact in the light curve. f, K2 photometry folded on the planet's orbital period with a transit model fit (red curve). BJD, barycentric Julian date.

$70M_{\oplus}$, corresponding to radial velocity semi-amplitudes of $5\text{--}56\text{ m s}^{-1}$. An even lower mass may be implied if the young planet is still undergoing Kelvin–Helmholtz radial contraction.

A semi-major axis of 0.04 AU ($\sim 8R_{*}$) is measured for K2-33 b from the orbital period and Kepler's third law, adopting the value of M_{*} in Table 1. The orbit is near the silicate dust sublimation radius, as well as the co-rotation radius, where some protoplanetary disk theories predict a magnetospheric cavity extending to the stellar surface²¹. At this separation, the blackbody equilibrium temperature of the planet is 850 K .

We have interpreted the observed transit as a single planet orbiting K2-33. Other interpretations involving eclipsing stellar binaries residing within the K2 aperture (Extended Data Fig. 4) would be diluted by the light of K2-33 and could potentially mimic the observed transit.

Table 1 | System properties of K2-33

Parameter	Value	Uncertainty
Stellar properties		
2MASS designation	J16101473–1919095	
EPIC designation	205117205	
Right ascension (J2000.0)	16 h 10 min 14.738 s	
Declination (J2000.0)	$-19^{\circ} 19' 09.55''$	
Proper motion, RA, μ_{α} (mas yr ⁻¹)	-9.8	± 1.7
Proper motion, dec., μ_{δ} (mas yr ⁻¹)	-24.2	± 1.8
Kepler magnitude, Kp (mag)	14.3	
Cluster distance, d (pc)	145	± 20
Kinematic distance, d_{kin} (pc)	139	± 11
Spectral type	M3	± 0.5
V-band extinction, A_V (mag)	1.29	
Luminosity, $\log(L_{*}/L_{\odot})$ (dex)	-0.83	± 0.07
Effective temperature, T_{eff} (K)	3,410	± 75
Stellar radius, R_{*} (R_{\odot})	1.1	± 0.1
Stellar mass, M_{*} (M_{\odot})	0.31	± 0.05
Mean stellar density, ρ_{*} (g cm ⁻³)	0.34	± 0.12
Surface gravity, $\log(g_{*})$ (dex)	3.84	± 0.16
Stellar rotation period, P_{rot} (days)	6.3	± 0.2
Systemic radial velocity, γ (km s ⁻¹)	-6.6	± 0.1
Projected rotational velocity, $v \sin(i)$ (km s ⁻¹)	5–9	
H α equivalent width (\AA)	-1.3	± 0.1
H β equivalent width (\AA)	-1.05	± 0.05
Li I 6,708 \AA equivalent width (\AA)	0.60	± 0.05
Light-curve modelling parameters		
Orbital period (days)	5.42513	$+0.00028$ -0.00029
Time of mid-transit, t_0 (BJD; days)	2,456,936.6665	$+0.0012$ -0.0012
Transit duration, T_{14} (hours)	4.22	$+0.15$ -0.10
Planet-to-star radius ratio, R_p/R_{*}	0.0476	$+0.0035$ -0.0017
Scaled semi-major axis, R_{*}/a	0.109	$+0.033$ -0.012
Impact parameter, b	0.49	$+0.26$ -0.33
Inclination, i (deg)	86.9	$+2.2$ -3.1
Mean stellar density, $\rho_{*,\text{circ}}$ (g cm ⁻³)	0.49	$+0.21$ -0.27
Linear limb darkening coefficient, u	0.603	$+0.052$ -0.053
Planet properties		
Planet radius, R_p (R_{\oplus})	5.76	$+0.62$ -0.58
Planet mass, M_p (M_{Jup})	<3.6	
Semi-major axis, a (AU)	0.0409	$+0.0021$ -0.0023
Blackbody equilibrium temperature, T_{eq} (K)	850	± 50

Right ascension and declination originate from 2MASS, proper motions from UCAC4, and Kepler magnitude from the Ecliptic Plane Input Catalog. The mean cluster distance³⁰ is assumed, with uncertainty equal to the presumed cluster depth¹². Quoted transit parameters and uncertainties are the medians and 15.87%, 84.13% percentiles of the posterior distributions.

Such a putative eclipsing stellar binary could be associated with (that is, gravitationally bound to) K2-33, or unassociated but aligned by chance. Given constraints from our suite of follow-up observations, we show that the chance of an eclipsing stellar binary producing the observed transit is vanishingly small.

We first consider unassociated eclipsing stellar binaries, which we characterize by their sky-projected separation from K2-33 and their brightness relative to K2-33 in the Kepler bandpass, ΔKp . Eclipse

depths may not exceed 100%; thus eclipsing stellar binaries with $\Delta Kp > 6.6$ mag cannot account for the 0.23% observed transit depth. We do not detect closely projected companions in seeing-limited and multi-epoch adaptive optics images (Extended Data Fig. 5), nor in searches for secondary lines in high-resolution optical spectra. These observational constraints, shown in Fig. 2a, eliminate nearly all scenarios involving unassociated eclipsing stellar binaries. The probability of an eclipsing stellar binary lurking in the remaining parameter space is $\ll 4 \times 10^{-6}$ (see Methods).

We now consider associated eclipsing stellar binaries in terms of their physical distance to K2-33, d , and ΔKp . As in the case of unassociated eclipsing stellar binaries, our imaging and spectroscopic data eliminate the vast majority of associated eclipsing stellar binary configurations. Additionally, the lack of detectable line-of-sight acceleration over the baseline of the observations rules out associated eclipsing stellar binaries in a mass-dependent manner (see Methods). The constraints provided by these complementary observations are depicted in Fig. 2b. However, some scenarios having $d = 1\text{--}3$ AU and $\Delta Kp = 2\text{--}6$ mag cannot be conclusively eliminated. Nearly all of these scenarios involve a planet orbiting either K2-33 or an undetected companion. If orbiting K2-33, the planet radius is at most 7.6% larger than the value reported in Table 1 (that is, within quoted uncertainties) owing to dilution from a companion. If orbiting a stellar or substellar companion to K2-33, the planet radius is at most $\sim 1.8M_{\text{Jup}}$, where M_{Jup} is the mass of Jupiter. Only for $\Delta Kp \geq 6$ mag does the radius of the transiting object correspond to a mass of $\geq 13M_{\text{Jup}}$ at 5–10 Myr. However, coeval eclipsing brown dwarfs probably would not produce eclipse depths $> 50\%$, and thus contrasts of $\Delta Kp \geq 5.8$ mag need not be considered. Furthermore, the low occurrence of brown dwarfs²² combined with the lack of observed secondary eclipses make such configurations extremely unlikely. Given the Kepler photometry and observational constraints, we quantitatively assessed the overall false-positive probability, using an established statistical framework²³ (see Methods). We found that scenarios involving a single star and planet are 10^{11} times more likely than scenarios involving eclipsing stellar binaries.

Spitzer Space Telescope observations of K2-33 revealed 24- μm emission in excess of the expected stellar photosphere by 50%, indicating the presence of cool circumstellar dust²⁴. There is an absence, however, of warm dust close to the star, given the lack of similar infrared excess at wavelengths shorter than 16 μm (ref. 25). The spectral energy distribution is best fitted by including a dust component at 122 K having an inner edge at 2.0 AU. These data suggest that the inner regions of the previously present protoplanetary disk have cleared. Supporting this inference is the modest H α signature (Table 1), which is consistent with chromospheric emission and indicates that the star is not accreting gas.

At the age of K2-33, it is unclear whether the dust structure consists of debris resulting from the collisional grinding of planetesimals, or whether it is a remnant of the initial dust- and gas-rich disk. One possibility is that the inner-disk regions have been cleared of dust by the gravitational influence of one or more planetary mass bodies²⁶. Our detection of a short-period planet in a transitional disk lends support to this explanation.

A flux upper limit at 880 μm from the Atacama Large Millimeter Array combined with the measured Spitzer fluxes yields a constraint on the mass of dust remaining in the disk of less than $0.2M_{\oplus}$ (ref. 27). Additionally, CO emission, a tracer of molecular hydrogen, was not detected²⁷, indicating that the primordial gas disk also has largely or entirely dissipated.

The transiting planet around the young star K2-33 provides direct evidence that large planets can be found at small orbital separations shortly after dispersal of the nebular gas. Migration via tidal circularization of an eccentric planet, through, for example, the Kozai–Lidov mechanism, planet–planet scattering, or secular chaos, proceeds over timescales much greater than disk dispersal timescales, and thus cannot explain the planet's current orbit. *In situ* formation, or formation

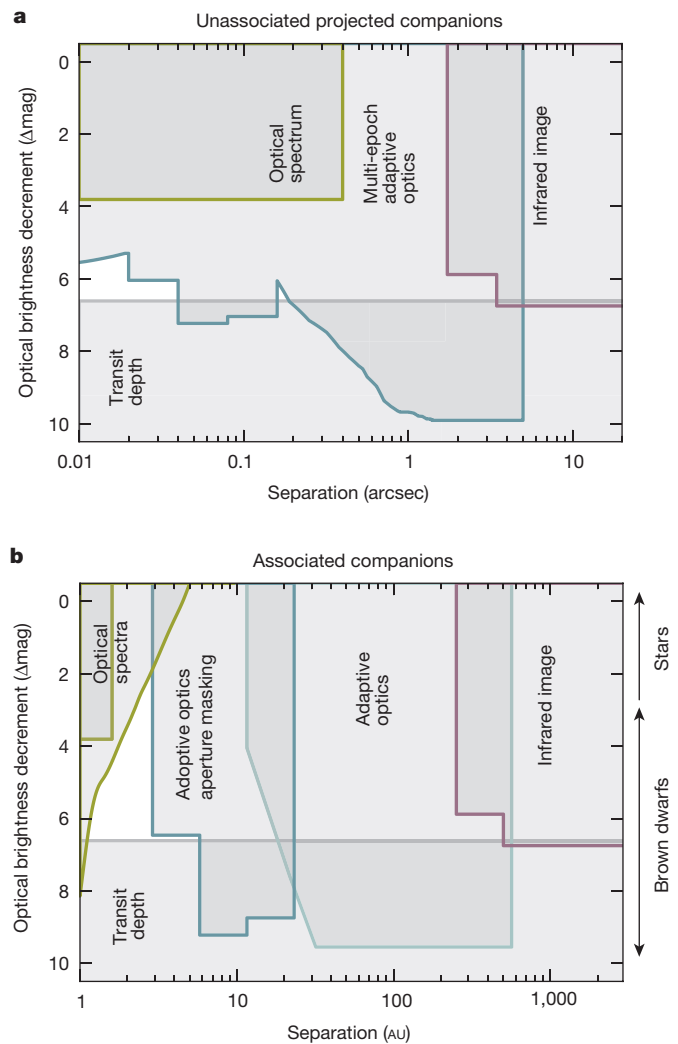


Figure 2 | Constraints on astrophysical false-positive scenarios.

To confirm the planetary nature of K2-33 b, we considered and eliminated nearly all false-positive scenarios involving eclipsing stellar binaries. **a**, The domain of sky-projected separation and contrast of a putative unassociated eclipsing stellar binary, aligned with K2-33 by chance. The blue outlined region shows eclipsing stellar binaries eliminated using multi-epoch adaptive optics imaging, which leverages stellar proper motion to provide sensitivity at all separations within $5''$. Green and purple regions represent constraints from optical spectra and seeing-limited imaging, respectively. Finally, eclipsing stellar binaries below the grey line cannot account for the observed transit depth and are eliminated. **b**, Limits on eclipsing stellar binaries associated with (that is, gravitationally bound to) K2-33. Constraints from imaging and spectroscopy are shown as a function of physical separation. The lack of detectable stellar acceleration provides an additional diagonal constraint at top left. Δmag , difference in magnitude.

at a larger separation followed by migration within the gas disk, are permitted scenarios given current observations.

Interestingly, large planets are rarely found close to mature low-mass stars; fewer than 1% of M-dwarfs host Neptune-sized planets with orbital periods of < 10 days²⁸, while $\sim 20\%$ host Earth-sized planets in the same period range²⁹. This may be a hint that K2-33 b is still contracting, losing atmosphere, or undergoing radial migration. Future observations may test these hypotheses, and potentially reveal where in the protoplanetary disk the planet formed.

Online Content Methods, along with any additional Extended Data display items and Source Data, are available in the online version of the paper; references unique to these sections appear only in the online paper.

Received 11 March; accepted 22 April 2016.

Published online 20 June 2016.

1. Kuiper, G. P. On the origin of the Solar System. *Proc. Natl Acad. Sci. USA* **37**, 1–14 (1951).
2. Kley, W. & Nelson, R. P. Planet-disk interaction and orbital evolution. *Annu. Rev. Astron. Astrophys.* **50**, 211–249 (2012).
3. Connelly, J. N. *et al.* The absolute chronology and thermal processing of solids in the solar protoplanetary disk. *Science* **338**, 651–655 (2012).
4. Lin, D. N. C., Bodenheimer, P. & Richardson, D. C. Orbital migration of the planetary companion of 51 Pegasi to its present location. *Nature* **380**, 606–607 (1996).
5. Rafikov, R. R. Atmospheres of protoplanetary cores: critical mass for nucleated instability. *Astrophys. J.* **648**, 666–682 (2006).
6. Hansen, B. M. S. & Murray, N. Migration then assembly: formation of Neptune-mass planets inside 1 AU. *Astrophys. J.* **751**, 158 (2012).
7. Chatterjee, S. & Tan, J. C. Inside-out planet formation. *Astrophys. J.* **780**, 53 (2014).
8. Boley, A. C., Granados Contreras, A. P. & Gladman, B. The *in situ* formation of giant planets at short orbital periods. *Astrophys. J.* **817**, L17 (2016).
9. Vanderburg, A. *et al.* Planetary candidates from the first year of the K2 mission. *Astrophys. J. Suppl. Ser.* **222**, 14 (2016).
10. Crossfield, I. J. M. *et al.* A nearby M star with three transiting super-Earths discovered by K2. *Astrophys. J.* **804**, 10 (2015).
11. Preibisch, T., Guenther, E. & Zinnecker, H. A large spectroscopic survey for young low-mass members of the Upper Scorpius OB association. *Astron. J.* **121**, 1040–1049 (2001).
12. Preibisch, T., Brown, A. G. A., Bridges, T., Guenther, E. & Zinnecker, H. Exploring the full stellar population of the Upper Scorpius OB association. *Astron. J.* **124**, 404–416 (2002).
13. Luhman, K. L. & Mamajek, E. E. The disk population of the Upper Scorpius association. *Astrophys. J.* **758**, 31 (2012).
14. McQuillan, A., Aigrain, S. & Mazeh, T. Measuring the rotation period distribution of field M dwarfs with Kepler. *Mon. Not. R. Astron. Soc.* **432**, 1203–1216 (2013).
15. Kurosawa, R., Harries, T. J. & Littlefair, S. P. Radial and rotational velocities of young brown dwarfs and very low-mass stars in the Upper Scorpius OB association and the ρ Ophiuchi cloud core. *Mon. Not. R. Astron. Soc.* **372**, 1879–1887 (2006).
16. Bouy, H. & Martín, E. L. Proper motions of cool and ultracool candidate members in the Upper Scorpius OB association. *Astron. Astrophys.* **504**, 981–990 (2009).
17. Herczeg, G. J. & Hillenbrand, L. A. Empirical isochrones for low mass stars in nearby young associations. *Astrophys. J.* **808**, 23 (2015).
18. Pecauc, M. J. & Mamajek, E. E. Intrinsic colors, temperatures, and bolometric corrections of pre-main-sequence stars. *Astrophys. J. Suppl. Ser.* **208**, 9 (2013).
19. Baraffe, I., Homeier, D., Allard, F. & Chabrier, G. New evolutionary models for pre-main sequence and main sequence low-mass stars down to the hydrogen-burning limit. *Astron. Astrophys.* **577**, A42 (2015).
20. Kraus, A. L. & Hillenbrand, L. A. The role of mass and environment in multiple-star formation: a 2MASS survey of wide multiplicity in three young associations. *Astrophys. J.* **662**, 413–430 (2007).
21. Armitage, P. J. Dynamics of protoplanetary disks. *Annu. Rev. Astron. Astrophys.* **49**, 195–236 (2011).
22. Bowler, B. P., Liu, M. C., Shkolnik, E. L. & Tamura, M. Planets around low-mass stars (PALMS). IV. The outer architecture of M dwarf planetary systems. *Astrophys. J. Suppl. Ser.* **216**, 7 (2014).
23. Morton, T. D. VESPA: false positive probabilities calculator. *Astrophys. Source Code Library* ascl:1503.011, <http://ascl.net/1503.011> (2015).
24. Carpenter, J. M., Mamajek, E. E., Hillenbrand, L. A. & Meyer, M. R. Debris disks in the Upper Scorpius OB association. *Astrophys. J.* **705**, 1646–1671 (2009).
25. Carpenter, J. M., Mamajek, E. E., Hillenbrand, L. A. & Meyer, M. R. Evidence for mass-dependent circumstellar disk evolution in the 5 Myr old Upper Scorpius OB association. *Astrophys. J.* **651**, L49–L52 (2006).
26. Trilling, D. E. *et al.* Debris disks around Sun-like stars. *Astrophys. J.* **674**, 1086–1105 (2008).
27. Barenfeld, S., Carpenter, J. M., Ricci, L. & Isella, A. ALMA observations of circumstellar disks in the Upper Scorpius OB association. *Astrophys. J.* (in the press); preprint at <https://arxiv.org/abs/1605.05772>.
28. Dressing, C. D. & Charbonneau, D. The occurrence rate of small planets around small stars. *Astrophys. J.* **767**, 95 (2013).
29. Dressing, C. D. & Charbonneau, D. The occurrence of potentially habitable planets orbiting M dwarfs estimated from the full Kepler dataset and an empirical measurement of the detection sensitivity. *Astrophys. J.* **807**, 45 (2015).
30. de Zeeuw, P. T., Hoogerwerf, R., de Bruijne, J. H. J., Brown, A. G. A. & Blaauw, A. A HIPPARCOS census of the nearby OB associations. *Astron. J.* **117**, 354–399 (1999).

Acknowledgements We thank S. Metchev, K. Batygin, B. Benneke, K. Deck, J. Fuller and A. Shporer for discussions, M. Ireland for software used in the aperture masking analysis, and A. Kraus for contributing to the 2011 Keck/NIRC2 data acquisition. T.J.D. is supported by an NSF Graduate Research Fellowship under Grant DGE1144469. E.A.P. is supported through a Hubble Fellowship. I.J.M.C. is supported through a Sagan Fellowship. A.W.H. acknowledges funding from NASA grant NNX16AE75G and NASA Research Support Agreement 1541779. This paper includes data collected by the Kepler mission, funded by the NASA Science Mission directorate. Some data presented here were obtained at the W. M. Keck Observatory, which is operated as a scientific partnership among the California Institute of Technology, the University of California and NASA. We acknowledge the important cultural role and reverence that the summit of Mauna Kea has always had within the indigenous Hawaiian community and we are fortunate to be able to conduct observations from this mountain.

Author Contributions T.J.D. noted the object as a young star, prepared the light curve, validated the transit, and led the overall analysis and the writing of the paper. L.A.H. analysed the 2015 and 2016 Keck/HIRES spectra, participated in team organization, performed general analysis, and contributed substantially to the writing of the paper. E.A.P. analysed raw K2 photometry and validated the transit, provided general guidance on exoplanets and false positives, and contributed substantially to the writing of the paper. J.M.C. was involved in the K2 proposal that included the object, and was principal investigator on the 2011 Keck/NIRC2, 2015 Keck/HIRES, and ALMA observations of the object. I.J.M.C. led the transit fitting and VESPA analysis. A.M.C. analysed the raw K2 photometry and validated the transit. A.W.H. and H.T.I. obtained, reduced, and analysed the 2016 Keck/HIRES spectra. D.R.C. led the clear aperture adaptive optics contrast curve analysis for the 2016 and 2011 data. C.A.B. wrote the proposal for 2016 Keck/NIRC2 follow-up of K2 sources and participated in the observations of the object. S.H. analysed the Keck/NIRC2 aperture masking data and assessed the temperature of the circumstellar dust. J.E.S. provided a rotational velocity analysis and calculated the kinematic distance. S.A.B. took the 2015 Keck/HIRES spectrum and analysed the ALMA data (referred to, but published separately in ref. 27).

Author Information Reprints and permissions information is available at www.nature.com/reprints. The authors declare no competing financial interests. Readers are welcome to comment on the online version of the paper. Correspondence and requests for materials should be addressed to T.J.D. (tjd@astro.caltech.edu).

Reviewer Information Nature thanks A. Collier Cameron and the other anonymous reviewer(s) for their contribution to the peer review of this work.

METHODS

Stellar membership and properties. The partial kinematics of K2-33 (Table 1) can be combined with the galactic velocity of the Upper Scorpius subgroup to estimate distance and predict radial velocity. We calculated these parameters following established methods³¹, adopting the mean UVW galactic velocities of the subgroup³², and estimated uncertainties using Monte Carlo sampling. We find $d_{\text{kin}} = 139 \pm 11$ pc, consistent with the mean subgroup distance from Earth 145 ± 2 pc (ref. 30), and radial velocity -7.3 ± 0.5 km s⁻¹, within 2σ of the systemic radial velocity we measure from multiple Keck/HIRES spectra (Extended Data Table 1).

We determined spectral type from the high-dispersion spectra and adopted an empirical spectral type to temperature conversion calibrated for young stars^{17,18} to estimate effective temperature (Table 1). From 2MASS photometry and the appropriate intrinsic $J-H$ colour for the spectral type¹⁸, we calculated the $J-H$ colour excess, $E(J-H) = 0.10$ mag. Assuming an extinction law we found visual and J-band extinctions of $A_V = 1.29$ mag and $A_J = 0.30$ mag, respectively. After correcting for extinction, we used the appropriate empirical J-band bolometric correction for the spectral type^{17,18} and a distribution of distances to calculate luminosity. While the mean association distance is known precisely, its large sky-projected area (about 150 deg²) suggests that the association depth is substantial. Results from a secular parallax study indicate an association distance spread of < 50 pc, with consideration of the angular diameter corresponding to a 35-pc spread^{12,33} at the mean distance. In calculating luminosity, we conservatively considered a uniform distribution of distances in a cubic volume 40 pc on each side, centred on the mean association distance of 145 pc (ref. 30). Uncertainty is calculated from Monte Carlo sampling, accounting for photometric errors, recommended errors in temperature¹⁷, and distance uncertainties. We propagated luminosity and temperature errors through in calculating the radius uncertainties using the Stefan–Boltzmann law.

Detailed modelling of the transit profile provides a constraint on mean stellar density, assuming a circular orbit³⁴. We found a mean stellar density of $\rho_{*,\text{circ}} = 0.49$ g cm⁻³, consistent with the value implied by our adopted M_* and R_* (Table 1). From the posterior distribution of mean stellar densities and a normal distribution in effective temperature, we interpolated between pre-main-sequence models¹⁹ to determine a stellar mass and age of $M_* = (0.30 \pm 0.04)M_\odot$ and $t = 5_{-2}^{+1}$ Myr, respectively (Extended Data Fig. 2). However, we conservatively adopt the ensemble age of the association, as we consider it more robust than the age of an individual star.

Stellar rotation and independent assessment of the stellar radius. We measured the stellar rotation period as $P_{\text{rot}} = 6.3 \pm 0.2$ days from a Lomb–Scargle periodogram^{35,36} of the light curve. Uncertainty was determined from the half-width at half-maximum of a Gaussian fit to the periodogram peak. Extended Data Fig. 1 depicts the light curve folded on the rotational period.

The stellar rotation speed as projected along the line of sight, $v \sin i_*$, was estimated from the spectra by artificially broadening an absorption spectrum of a slowly rotating stellar template of similar temperature to K2-33, acquired using the same spectrograph and set-up. The range of plausible rotational velocities is constrained through minimization of the residuals between the broadened template and the observed spectrum. We find a most likely projected rotation velocity $v \sin i_* \approx 5\text{--}9$ km s⁻¹. Combined with the rotation period measured from the light curve, we used the projected rotational velocity to determine an independent estimate of the stellar radius modulated by the sine of the stellar inclination of $R_* \sin i_* = v \sin i_* \cdot P_{\text{rot}} / 2\pi = (0.85 \pm 0.25)R_\odot$, where we quote a 95% confidence interval assuming a uniform distribution in $v \sin i_*$.

Our value for $R_* \sin i_*$ is consistent with the Stefan–Boltzmann radius within 2σ . Two effects could bias $R_* \sin i_*$ away from the true value of R_* : (1) the surface features dominating the rotational modulation of the light curve may be confined to a range of stellar latitudes that may not reflect the same velocity field encoded in the rotational broadening of spectral lines, and (2) the star may have an inclination resulting in the value of $\sin i_*$ being substantially < 1 . If this is the case, the orbit of K2-33 b is misaligned with the spin of its host star. While $R_* \sin i_*$ provides a valuable consistency check on stellar radius, we use the Stefan–Boltzmann radius given its insensitivity to the unknown stellar inclination.

K2 time series photometry treatment. The K2 mission³⁷ observes fields along the ecliptic plane for approximately 75 days at a time. K2 photometry possesses percentage-level systematic signatures from pointing drift and intra-pixel detector sensitivity variations that must be corrected in order to detect sub-per-cent planet transits. We acquired such a corrected light curve from the Exoplanet Follow-up Observing Program public website⁹, derived using a $12'' \times 16''$ rectangular aperture (Extended Data Fig. 4).

Before modelling the transit profile, we removed the spot modulation pattern using a cubic basis spline fit with knots spaced by 12 long-cadence measurements,

employing iterative rejection of outliers³⁸. We verified that no in-transit observations were included in the spline fit by phasing the flattened light curve on the orbital period and inspecting the points excluded from the fit. An artificial gap in the systematics-corrected light curve from the ExoFOP page was not adequately captured by the spline fit and, consequently, we excluded from further analysis those data with BJD values in the range 2,456,936 to 2,456,938, resulting in the loss of a single transit. We assigned a constant observational uncertainty for each K2 measurement, determined from the standard deviation in the out-of-transit light curve (here defined as observations more than 12 h from either side of the transit centres).

Transit model-fitting analysis. We employed previously established methodology¹⁰ for fitting transit models to the light curve. The approach uses the BATMAN software³⁹ (<https://pppi.python.org/pppi/batman-package/2.1.0>), based on the Mandel and Agol analytic light-curve formalism⁴⁰, to generate model transit profiles. Transit models were numerically integrated to match the ~ 30 -min cadence of K2 observations. We assumed a linear limb-darkening law for the star, imposing a Gaussian prior on the linear limb-darkening coefficient, u , based on tabulated values⁴¹ appropriate for the effective temperature and surface gravity of K2-33. We also allowed for dilution by light from a second star in the fitting. In post-processing, we selected only those samples corresponding to dilution levels consistent with our companion exclusion analysis (Fig. 2).

The directly fitted transit parameters are the scaled semi-major axis (a/R_*), the planet-to-star radius ratio (R_p/R_*), the orbital period (P), the time of mid-transit (t_0) and the inclination (i). The multi-dimensional transit parameter space was explored using an affine invariant implementation of the Markov chain Monte Carlo algorithm⁴² to find the best-fit model and determine parameter uncertainties. Each observation was weighted equally, resulting in a best-fit likelihood of $-1/2 \times \chi^2$. We followed established methods¹⁰ for Markov chain Monte Carlo initialization, burn-in treatment, rescaling of data weights, and convergence testing. Table 1 quotes median transit model values, with uncertainties determined from the 15.87% and 84.13% percentiles of the parameter posterior distributions.

The scatter in transit is $\sim 15\%$ larger than the scatter in equal duration intervals before and after transit. One possible explanation may be spot-crossing events, given that the star is expected to have a high spot-covering fraction⁴³, supported by the modulation in the unflattened light curve.

Prior to adopting the publicly available light curve⁹, we independently extracted a light curve from K2 target pixel files using a different photometric pipeline^{10,44}. Performing the same modelling described above on this second light curve produced consistent results.

High-spectral-resolution observations and radial velocities. We used the High Resolution Spectrograph⁴⁵ (HIRES) on the 10-m Keck-1 telescope to measure the radial velocity of K2-33 relative to the Solar System barycentre (Extended Data Table 1) to confirm its cluster membership, and to constrain the mass of K2-33 b. The resolution of these spectra are $R \approx 50,000$ in the range $\sim 3,600\text{--}8,000$ Å for the 2016 epochs and $R \approx 36,000$ in the range $\sim 4,800\text{--}9,200$ Å for the 2015 epoch.

For the first epoch, velocity was derived by cross-correlating the spectrum with radial velocity standards⁴⁶ observed using HIRES in the same spectrograph configuration. Uncertainty is quantified from the dispersion among measurements relative to different standards, and over many different spectral orders. For the three epochs in 2016, systemic radial velocity was measured using the telluric A and B absorption bands as a fiducial wavelength reference. Assessing all measurements, the star's systemic radial velocity is -6.6 ± 0.1 km s⁻¹, where we quote a weighted average and standard deviation.

Limits on companions from the spectroscopic data. We searched for and excluded distant gravitationally bound companions to K2-33 by looking for trends in the 265-day radial velocity time series. A 3σ upper limit to any possible acceleration is 2.6 km s⁻¹ yr⁻¹. Following established methods⁴⁷, the limiting minimum mass detectable from the radial velocity measurements as a function of orbital separation rules out additional companions of $\geq 0.14M_\odot$ at 3 AU and $\geq 0.39M_\odot$ at 5 AU.

We also searched for secondary spectral lines⁴⁸ that would arise from a companion projected within $0.4''$ of the primary. No stars as faint as 3% of the brightness of the primary were detected, though we are blind to companion stars with a small (< 15 km s⁻¹) radial velocity relative to the primary because the spectral lines of the two stars would not be distinguished.

High-resolution imaging. Using adaptive optics at the Keck-2 telescope on UTC 2011 May 15, we obtained ten 9-s exposures of K2-33. A second set of Keck/NIRC2 images was acquired on UTC 2016 February 17 in a three-point dither pattern with 10-s integrations per dither position, repeated three times. For both epochs, the narrow-camera optics were used resulting in a pixel scale of 9.942 mas per pixel; the final co-added images have a resolution of $0.07''$ (full-width at half-maximum). The observations at the two epochs have the same total integration time, so the final images have comparable depth.

To estimate sensitivity to point sources as a function of radial distance from the star, median flux levels and root-mean-square dispersions (σ) were calculated in incremental annuli centred on the source. An image was constructed with these characteristics and synthetic sources with full-width at half-maximum equivalent to that of K2-33 were injected into the image at varying positions and brightnesses. The synthetic sources were then measured to determine the 5σ detection limit. Comparing the instrumental magnitude to that of the star produces ΔK for that annulus.

Non-redundant aperture masking. K2-33 was observed using an aperture mask on the same 2011 night as the clear aperture images were taken. Aperture masking interferometry⁴⁹ uses an opaque mask with clear holes such that the baseline between any two samples a unique spatial frequency in the pupil plane, and achieves angular resolution as good as $1/3 \times \lambda/D$ compared to $1.2 \times \lambda/D$, though at the expense of diminished throughput^{50,51}.

With the nine-hole mask in the NIRC2 camera, we obtained 40 dithered images using 20-s exposures. Observations of calibrator stars were interspersed with the targets and obtained in an identical manner. In each image, the mask creates a set of 36 overlapping interference fringes on the detector. The bispectrum, the complex triple product of visibilities defined by the three baselines formed from any three subapertures, is then calculated. The phase of this complex quantity is the closure phase, which has the advantage of being largely insensitive to phase delays owing to atmospheric effects or residual uncorrected phase aberrations not sensed by the adaptive optics system. We followed established procedures^{52,53} for calculating the closure phase for calibrator stars.

Limits on companions from the imaging data. Using all three sets of high-spatial-resolution near-infrared imaging data, we searched for projected companions to K2-33 (either gravitationally bound or foreground/background sources). The two epochs of clear aperture data each achieved $\Delta K > 4.5$ mag of contrast beyond $0.13''$ and $\Delta K > 7.5$ mag beyond $1''$. In the interim between the observations, K2-33 moved on the sky by $0.1228'' \pm 0.0085''$ owing to its parallactic and proper motion. The combined set of infrared images thus rules out nearly all unassociated background stars bright enough to produce the transit observed in the optical. The aperture masking observations are sensitive to more closely projected (from $0.02''$ – $0.16''$) companions in the stellar and substellar mass regimes. We use these to rule out potential associated companions larger than 19 Jupiter masses down to orbital separations of 3 AU, and are sensitive to companions with masses as low as 11–12 Jupiter masses in the range 6–23 AU, where quoted companion masses are model-dependent¹⁹ conservatively assuming an age of 10 Myr. Finally, a prior analysis⁵⁴ of near-infrared photometry ruled out associated companions down to masses of 5%–6% of the primary mass at separations of $1.7''$ – $27.5''$, or approximately 250–4,000 AU.

The imaging limits constrain the brightnesses of any putative companions in the near-infrared K-band. To approximately convert these contrast limits to constraints in the optical Kepler bandpass, Kp , we employed a combination of theoretical evolutionary models and empirical colour–colour relations. The TRILEGAL simulation discussed below predicts that the mean potential contaminant towards K2-33 would have infrared colour $J - K_s = 0.57$ mag, corresponding to a K-type dwarf. From an empirical optical–infrared Kp -to- K_s conversion⁵⁵, we conclude that a typical contaminating source would have colour $Kp - K_s = 2.00$ mag. We thus gain an additional 2 magnitudes of contrast when converting the NIRC2 contrast curve to the corresponding limits in the Kepler bandpass when considering unassociated companions.

For associated companions, the imaging constraints natively derived in the near-infrared were converted to optical limits using pre-main-sequence evolutionary models¹⁹. Putative companion masses can be paired with our assumed primary mass to yield predicted R-band contrasts at 5–10 Myr, where the R-band serves as a proxy for the Kepler bandpass. Notably, for the clear aperture adaptive optics region of Fig. 2b, the contrast achieved beyond 30 AU is better than represented in the figure owing to limitations of the models, which do not extend below $10M_{\text{Jup}}$ (corresponding to $\Delta Kp \geq 9.5$ mag).

We rule out nearly all stellar and brown-dwarf mass companions to K2-33, with the exception of a narrow swath of parameter space corresponding to ultra-low-mass stars or brown dwarfs separated by 1–3 AU from the primary (Fig. 2). The physically permitted (as opposed to unexcluded) separation range of any hypothetical diluting companion is even smaller, considering that the inferred inner edge of the disk is at 2 AU.

Galactic structure model and intracluster contamination. In addition to searching directly for sources that could contaminate the K2 light curve, we estimated the expected surface density of such sources as a function of magnitude using the TRILEGAL version 1.6 model^{56,57} (<http://stev.oapd.inaf.it/cgi-bin/trilegal>) of the Milky Way Galaxy. Notably, TRILEGAL does not include the local extinction due to gas and dust associated with Upper Scorpius itself, and therefore produces an upper limit to the field-star source density. We simulated a 1-deg^2 field and scaled

the resulting numbers first to the 10×10 arcsec² field of view of the Keck/NIRC2 images and the 12×16 arcsec² K2 photometric aperture, and then to the unexcluded regions of parameter space in Fig. 2a. We found the TRILEGAL prediction for the expected surface density of sources to the $K_s < 18.0$ mag limit (5σ) of the NIRC2 data, and translated it to < 0.15 sources per NIRC2 field, consistent with our detection of none. Within the K2 photometry aperture, < 0.3 unassociated sources are expected to the same magnitude limit, corresponding to a mean optical brightness of $Kp = 18.6$ mag.

By considering the surface density of sources expected from integrating essentially all the way through the galaxy, a maximum of three sources are expected in the K2 aperture, having mean optical brightness $Kp = 23.1$ mag, which is too faint to explain the transit depth. Indeed, we have ruled out nearly all companions with projected separations larger than $0.04''$, as well as effectively all of those inside $0.04''$; fewer than 4×10^{-6} sources are expected in the remaining unexcluded parameter space of Fig. 2a. An even smaller number of sources are expected to be eclipsing stellar binaries. Therefore, in addition to not detecting any contaminants in the high-spatial-resolution imaging and spectroscopic data, we argue that essentially none are expected.

A similar source-density argument can be used to constrain the probability of contaminants with nearly identical proper motions to K2-33, probably association members that are foreground or background to K2-33. The multi-epoch adaptive optics imaging cannot rule out closely projected sources within $0.02''$ (the inner limit probed by the aperture masking observations) that are also co-moving with K2-33 between 2011 and 2016. From the observed Upper Scorpius mass function and width of the association on the sky¹², we estimated a source density of about 16 members deg⁻². Thus, fewer than 2×10^{-9} co-moving contaminants are expected within $0.02''$ of K2-33.

False-positive probability analysis. Eclipsing stellar binaries, when diluted by the light of a third star, can produce light curves that masquerade as a planetary transit. These false positives come in three broad classes: (1) undiluted eclipsing stellar binaries, (2) background (and foreground) eclipsing stellar binaries where the eclipses are diluted by the target star, and (3) bound eclipsing stellar binaries in hierarchical triple systems.

We used the VESPA program²³ (<https://pypi.python.org/pypi/VESPA/0.4.7>) to compare the likelihood of each binary scenario against the planetary interpretation. As input for the calculation, we provide the K2 light curve, the stellar parameters, and to be as conservative as possible, we adopt our least stringent imaging constraints: the 2011 NIRC2 clear contrast curve, and the aperture masking limits. Even in this minimally constraining scenario, we find a false-positive probability of $< 1 \times 10^{-11}$ from VESPA, as expected given our exclusion in Fig. 2 of essentially all the modelled scenarios. Notably, however, VESPA does not account for substellar objects, pre-main-sequence evolution, extinction, or the unknown prior probability of planets around 5–10-Myr-old stars.

Implications of hierarchical triple scenarios. The conjectured hierarchical triple configuration is argued elsewhere as unlikely on the basis of population statistics; however, we must still consider the possibility that K2-33 b has a larger radius owing to dilution of the transit depth by a luminous companion to K2-33. We first consider the case in which the planet orbits K2-33, but the transit depth is diluted by an undetected secondary. In this scenario, the ratio of the true planet radius to the observed planet radius (that is, not accounting for dilution) is $R_{\text{p,true}}/R_{\text{p,obs}} = \sqrt{1 + F_{\text{sec}}/F_{\text{pri}}}$, where $F_{\text{sec}}/F_{\text{pri}}$ is the optical flux ratio between the secondary and primary. For ΔKp in the range 2–6 mag, the true planet radius is at most 7.6% larger, within our quoted uncertainties.

Now, we consider the case in which the planet orbits an undetected companion to K2-33. In this scenario, the planet radius is $R_p = R_{\text{sec}} \sqrt{\delta_0(1 + F_{\text{pri}}/F_{\text{sec}})}$, where R_{sec} is the secondary radius, and δ_0 is the observed transit depth. Using ΔR as a proxy for ΔKp , we found the secondary radius implied by the optical brightness decrement using evolutionary models¹⁹ valid for 5–10 Myr. For ΔKp in the range 2–6 mag, we found that the implied planet radius is in the range $(0.56\text{--}1.85)R_{\text{Jup}}$. At these ages, such radii correspond to planet masses of $\leq 13M_{\text{Jup}}$. Only for $\Delta Kp \geq 6$ mag does the implied mass exceed the nominal brown-dwarf minimum mass. However, coeval eclipsing brown dwarfs are unlikely to produce eclipse depths of $> 50\%$ (corresponding to contrasts of $\Delta Kp \geq 5.8$ mag). Furthermore, we argue that scenarios involving eclipsing brown dwarfs 1–3 AU from K2-33 are extremely unlikely, for several compounding reasons: (1) the observed frequency of brown-dwarf companions to M-dwarfs is a few per cent^{22,58}; (2) in the restricted domain of $a = 1\text{--}3$ AU, the frequency is lower still; and (3) the frequency of eclipsing brown dwarf pairs so similar in size and temperature that the primary and secondary eclipses are indistinguishable is smaller still. Finally, the tenuous dust disk with inner edge at 2 AU is further evidence in favour of the single-star scenario.

Cluster age. The age of Upper Scorpius is constrained to be 5–10 Myr, from a variety of considerations. Absence of dense molecular gas or protostars in Upper

Scorpius implies that star formation has ceased in the region⁵⁹, while the presence of protoplanetary disks around a significant fraction of members indicates that planet formation is ongoing¹³. However, the precise age of the association is currently debated. An early kinematic analysis, in which the motions of high-mass members were traced back in time to the point of closest proximity to one another, suggested an age of 5 Myr (ref. 60). The first Hertzsprung–Russell diagram analysis of the full stellar population, spanning from the highest to the lowest masses, also determined an age of 5 Myr without appreciable dispersion¹². Most subsequent age determinations using theoretical evolutionary models in the Hertzsprung–Russell diagram arrived at the same consistent age of 5–6 Myr for massive main-sequence turnoff stars^{61,62}, low-mass stars^{17,63–65}, as well as substellar mass objects⁶⁶.

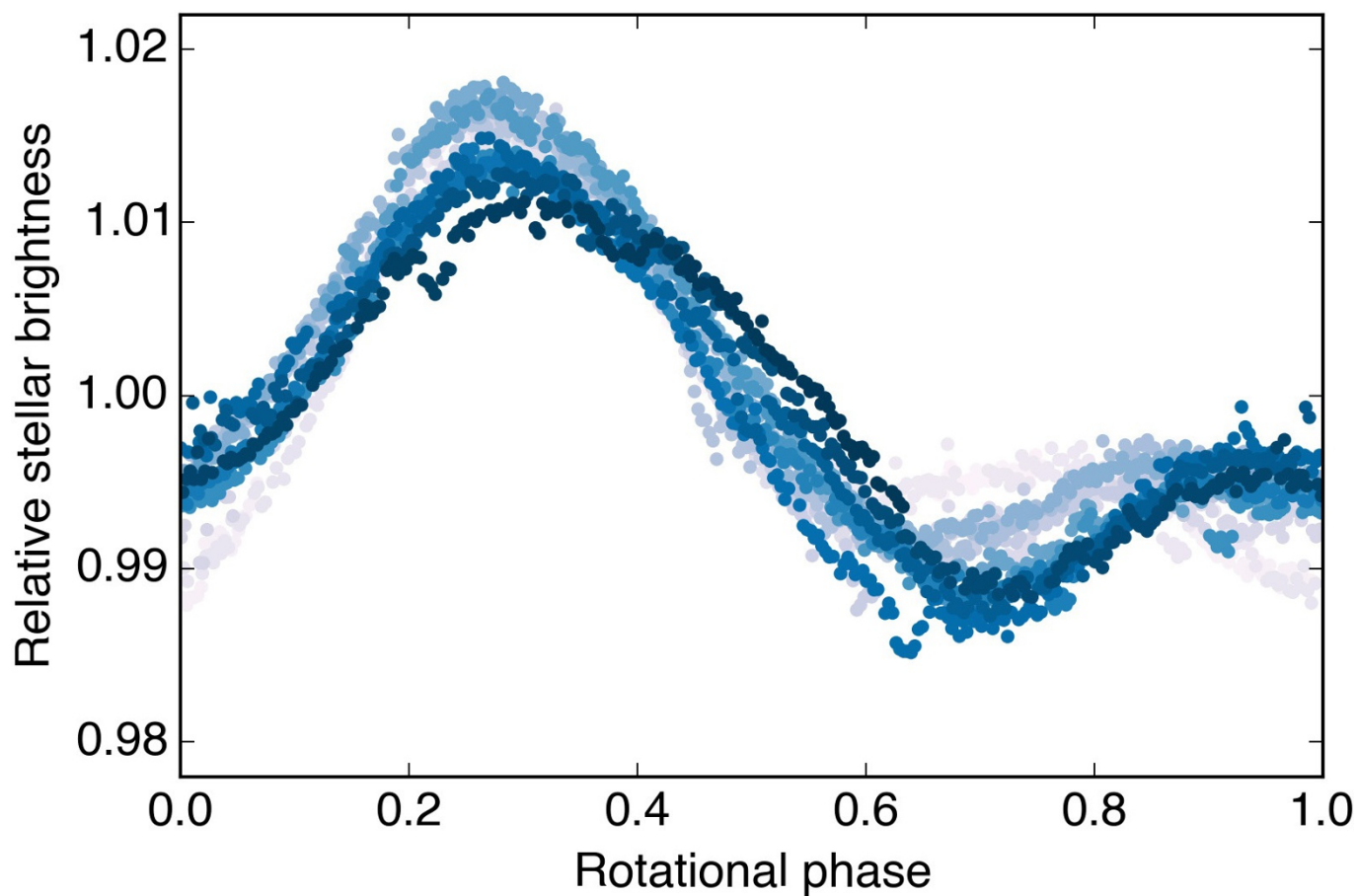
However, the association age has also been determined to be closer to 10 Myr from analyses of low-mass members^{67,68} and the intermediate-mass pre-main-sequence and main-sequence population, main-sequence turn-off stars, and the supergiant Antares⁶⁹. Emerging evidence from double-lined eclipsing binaries also supports an age in the range of 7–11 Myr^{38,70,71}, as does an updated kinematic analysis⁶⁹. Despite the lack of consensus on the precise age of Upper Scorpius, the full error-inclusive range of estimates in the literature (3–13 Myr) place the association at a critically important stage in the planet formation process—when most primordial disks have dispersed⁷².

K2-33 b in the context of other claimed young planets. While several secure short-period planets have been found in orbit around stars in benchmark open clusters including the 600–800-Myr-old Hyades^{73,74} and Praesepe^{75,76}, the evidence for planets at younger ages is mixed. Direct imaging has revealed (5–10) M_{Jup} ‘planetary mass companions’ located at large semi-major axes from several stars having ages of a few tens to a few hundreds of million years. Additionally, there are strong indications of ongoing planet formation in many 1–3-Myr-old circumstellar disks, based on the observed radial structure of dust.

However, there are no confirmed planets in the Jupiter or sub-Jupiter mass range with ages less than those corresponding to the late-heavy-bombardment era in our own Solar System. Both TW Hya and PTFO 8–8695 have been claimed to host hot Jupiter candidates detected via radial velocity or transit methods, but neither object has stood up to scrutiny^{77–79}. K2-33 b at an age of 5–10 Myr, in contrast, is a secure transiting planet. It is slightly larger than Neptune and its mass is probably similar to Neptune’s mass.

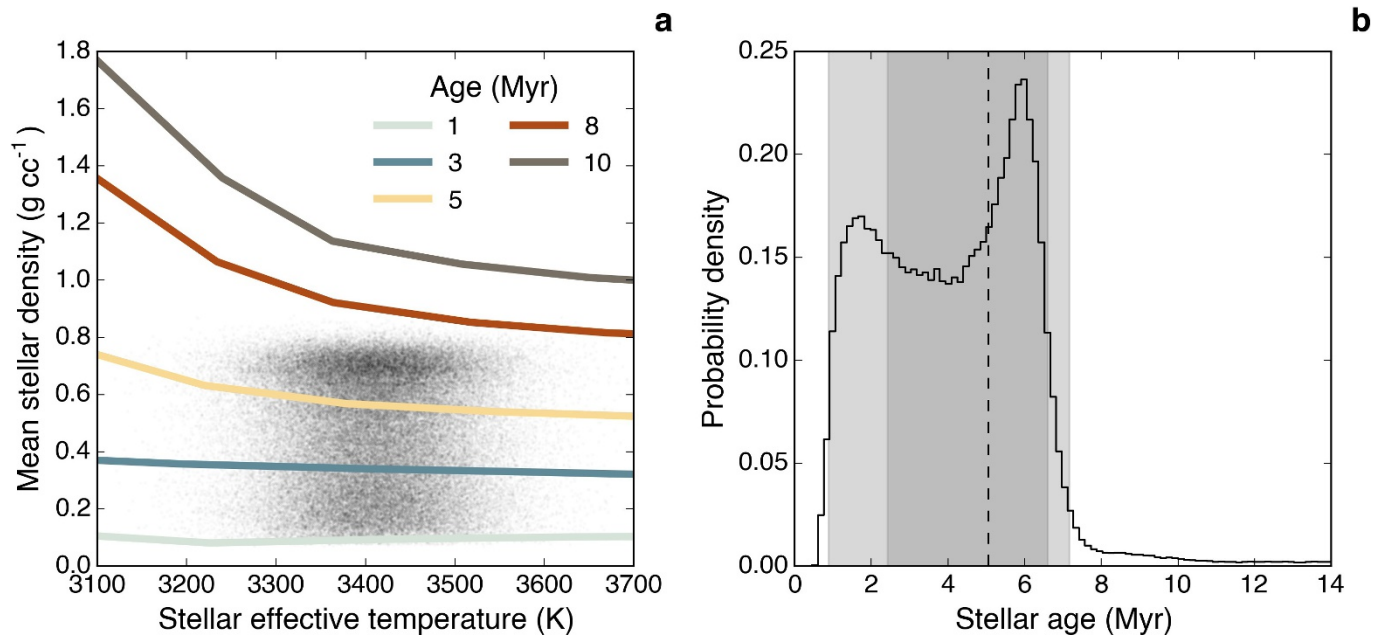
Code availability. We have opted not to make available our custom codes employed in the various elements of our data reduction and analysis, as they are either not of general purpose use, lack sufficient documentation, or they are already publicly available. The results of the computer processing are provided as Source Data. The raw data are publicly available, either currently (K2) or after a limited proprietary period (Keck, ALMA).

31. Lépine, S. & Simon, M. Nearby young stars selected by proper motion. I. Four new members of the β Pictoris moving group from the Tycho-2 catalog. *Astron. J.* **137**, 3632–3645 (2009).
32. Chen, C. H. *et al.* A Magellan MIKE and Spitzer MIPS study of 1.5–1.0 M_{\odot} stars in Scorpius-Centaurus. *Astrophys. J.* **738**, 122 (2011).
33. de Bruijne, J. H. J. Structure and colour-magnitude diagrams of Scorpius OB2 based on kinematic modelling of Hipparcos data. *Mon. Not. R. Astron. Soc.* **310**, 585–617 (1999).
34. Seager, S. & Mallén-Ornelas, G. A unique solution of planet and star parameters from an extrasolar planet transit light curve. *Astrophys. J.* **585**, 1038–1055 (2003).
35. Lomb, N. R. Least-squares frequency analysis of unequally spaced data. *Astrophys. Space Sci.* **39**, 447–462 (1976).
36. Scargle, J. D. Studies in astronomical time series analysis. II—Statistical aspects of spectral analysis of unevenly spaced data. *Astrophys. J.* **263**, 835–853 (1982).
37. Howell, S. B. *et al.* The K2 mission: characterization and early results. *Publ. Astron. Soc. Pacif.* **126**, 398–408 (2014).
38. David, T. J., Hillenbrand, L. A., Cody, A. M., Carpenter, J. M. & Howard, A. W. K2 discovery of young eclipsing binaries in Upper Scorpius: direct mass and radius determinations for the lowest mass stars and initial characterization of an eclipsing brown dwarf binary. *Astrophys. J.* **816**, 21 (2015).
39. Kreidberg, L. BATMAN: BASIC Transit Model cAlculationN in Python. *Publ. Astron. Soc. Pacif.* **127**, 1161–1165 (2015).
40. Mandel, K. & Agol, E. Analytic light curves for planetary transit searches. *Astrophys. J.* **580**, L171–L175 (2002).
41. Claret, A., Hauschildt, P. H. & Witte, S. New limb-darkening coefficients for PHOENIX/1D model atmospheres. I. Calculations for $1500 K \leq T_{\text{eff}} \leq 4800 K$ Kepler, CoRot, Spitzer, uvby, UVRIJKH, Sloan, and 2MASS photometric systems. *Astron. Astrophys.* **546**, A14 (2012).
42. Foreman-Mackey, D., Hogg, D. W., Lang, D. & Goodman, J. emcee: the MCMC hammer. *Publ. Astron. Soc. Pacif.* **125**, 306–312 (2013).
43. Jackson, R. J. & Jeffries, R. D. The effect of starspots on the radii of low-mass pre-main-sequence stars. *Mon. Not. R. Astron. Soc.* **441**, 2111–2123 (2014).
44. Petigura, E. A. *et al.* Two transiting Earth-size planets near resonance orbiting a nearby cool star. *Astrophys. J.* **811**, 102 (2015).
45. Vogt, S. S. *et al.* in *Instrumentation in Astronomy VIII* (eds Crawford, D. L. & Craine, E. R.) *Proceedings of SPIE* Vol. 2198, 362–375, <http://proceedings.spiedigitallibrary.org/proceeding.aspx?articleid=959834> (SPIE, 1994).
46. Nidever, D. L., Marcy, G. W., Butler, R. P., Fischer, D. A. & Vogt, S. S. Radial velocities for 889 late-type stars. *Astrophys. J. Suppl. Ser.* **141**, 503–522 (2002).
47. Montet, B. T., Crepp, J. R., Johnson, J. A., Howard, A. W. & Marcy, G. W. The TRENDS high-contrast imaging survey. IV. The occurrence rate of giant planets around M dwarfs. *Astrophys. J.* **781**, 28 (2014).
48. Kolbl, R., Marcy, G. W., Isaacson, H. & Howard, A. W. Detection of stars within $\sim 0.8''$ of Kepler objects of interest. *Astron. J.* **149**, 18 (2014).
49. Tuthill, P. G., Monnier, J. D., Danchi, W. C., Wishnow, E. H. & Haniff, C. A. Michelson interferometry with the Keck I telescope. *Publ. Astron. Soc. Pacif.* **112**, 555–565 (2000).
50. Baldwin, J. E., Haniff, C. A., Mackay, C. D. & Warner, P. J. Closure phase in high-resolution optical imaging. *Nature* **320**, 595–597 (1986).
51. Readhead, A. C. S. *et al.* Diffraction-limited imaging with ground-based optical telescopes. *Astron. J.* **95**, 1278–1296 (1988).
52. Kraus, A. L., Ireland, M. J., Martinache, F. & Hillenbrand, L. A. Mapping the shores of the brown dwarf desert. II. Multiple star formation in Taurus-Auriga. *Astrophys. J.* **731**, 8 (2011).
53. Hinkley, S. *et al.* Discovery of seven companions to intermediate-mass stars with extreme mass ratios in the Scorpius-Centaurus association. *Astrophys. J.* **806**, L9 (2015).
54. Kraus, A. L. & Hillenbrand, L. A. Multiple star formation to the bottom of the initial mass function. *Astrophys. J.* **757**, 141 (2012).
55. Howell, S. B. *et al.* Kepler-21b: a 1.6 R_{Earth} planet transiting the bright oscillating F subgiant star HD 179070. *Astrophys. J.* **746**, 123 (2012).
56. Girardi, L., Groenewegen, M. A. T., Hatziminaoglou, E. & da Costa, L. Star counts in the Galaxy. Simulating from very deep to very shallow photometric surveys with the TRILEGAL code. *Astron. Astrophys.* **436**, 895–915 (2005).
57. Girardi, L. *et al.* TRILEGAL, a TRIdimensional model of the GALaxy: status and future. *Astrophys. Space Sci. Proc.* **26**, 165–170 (2012).
58. Dieterich, S. B., Henry, T. J., Golimowski, D. A., Krist, J. E. & Tanner, A. M. The solar neighborhood. XXVIII. The multiplicity fraction of nearby stars from 5 to 70 AU and the brown dwarf desert around M dwarfs. *Astron. J.* **144**, 64 (2012).
59. Preibisch, T. & Mamajek, E. *The Nearest OB Association: Scorpius-Centaurus (Sco OB2)* (ed. Reipurth, B.) 235–284, <http://aspmonographs.org/custom/publications/paper/005-0235.html> (Astronomical Society of the Pacific Monograph Publications, 2008).
60. Blaauw, A. in *NATO Advanced Science Institutes Series C* (eds Lada, C. J. & Kylafis, N. D.) Vol. 342, 125–154 (ASI, 1991).
61. de Zeeuw, T. & Brand, J. in *Birth and Evolution of Massive Stars and Stellar Groups* (eds Boland, W. & van Woerden, H.) *Astrophysics and Space Science Library* Vol. 120, 95–101 (Springer, 1985).
62. de Geus, E. J., de Zeeuw, P. T. & Lub, J. Physical parameters of stars in the Scorpio-Centaurus OB association. *Astron. Astrophys.* **216**, 44–61 (1989).
63. Preibisch, T. & Zinnecker, H. The history of low-mass star formation in the Upper Scorpius OB association. *Astron. J.* **117**, 2381–2397 (1999).
64. Slesnick, C. L., Hillenbrand, L. A. & Carpenter, J. M. A large-area search for low-mass objects in Upper Scorpius. II. Age and mass distributions. *Astrophys. J.* **688**, 377–397 (2008).
65. Lodieu, N., Dobbie, P. D. & Hambly, N. C. Multi-fibre optical spectroscopy of low-mass stars and brown dwarfs in Upper Scorpius. *Astron. Astrophys.* **527**, A24 (2011).
66. Allen, P. R., Trilling, D. E., Koerner, D. W. & Reid, I. N. Luminosity functions of young clusters: modeling the substellar mass regime. *Astrophys. J.* **595**, 1222–1230 (2003).
67. Martin, E. L. Weak and post-T Tauri stars around B-type members of the Scorpius-Centaurus OB association. *Astron. J.* **115**, 351–357 (1998).
68. Frink, S. *Kinematics of T Tauri Stars in Nearby Star Forming Regions*. PhD thesis, Astronomisches Rechen-Institut Heidelberg (1999); <http://adsabs.harvard.edu/abs/1999PhDT.....9F>.
69. Pecaut, M. J., Mamajek, E. E. & Bubar, E. J. A revised age for Upper Scorpius and the star formation history among the F-type members of the Scorpius-Centaurus OB association. *Astrophys. J.* **746**, 154 (2012).
70. Kraus, A. L. *et al.* The mass-radius relation of young stars. I. USco 5, an M4.5 eclipsing binary in Upper Scorpius observed by K2. *Astrophys. J.* **807**, 3 (2015).
71. Lodieu, N. *et al.* An eclipsing double-line spectroscopic binary at the stellar/substellar boundary in the Upper Scorpius OB association. *Astron. Astrophys.* **584**, A128 (2015).
72. Wyatt, M. C. Evolution of debris disks. *Annu. Rev. Astron. Astrophys.* **46**, 339–383 (2008).
73. Mann, A. W. *et al.* Zodiacal exoplanets in time (ZEIT). I. A Neptune-sized planet orbiting an M4.5 dwarf in the Hyades Star Cluster. *Astrophys. J.* **818**, 46 (2016).
74. David, T. J. *et al.* New Pleiades eclipsing binaries and a Hyades transiting system identified by K2. *Astron. J.* **151**, 112 (2016).
75. Quinn, S. N. *et al.* Two “b”s in the beehive: the discovery of the first hot Jupiters in an open cluster. *Astrophys. J.* **756**, L33 (2012).
76. Malavolta, L. *et al.* The GAPS programme with HARPS-N at TNG. XI. Pr 0211 in M 44: the first multi-planet system in an open cluster. *Astron. Astrophys.* **588**, A118 (2016).
77. Rucinski, S. M. *et al.* Photometric variability of the T Tauri star TW Hya on time-scales of hours to years. *Mon. Not. R. Astron. Soc.* **391**, 1913–1924 (2008).
78. Huéramo, N. *et al.* TW Hydrae: evidence of stellar spots instead of a hot Jupiter. *Astron. Astrophys.* **489**, L9–L13 (2008).
79. Yu, L. *et al.* Tests of the planetary hypothesis for PTFO 8-8695b. *Astrophys. J.* **812**, 48 (2015).



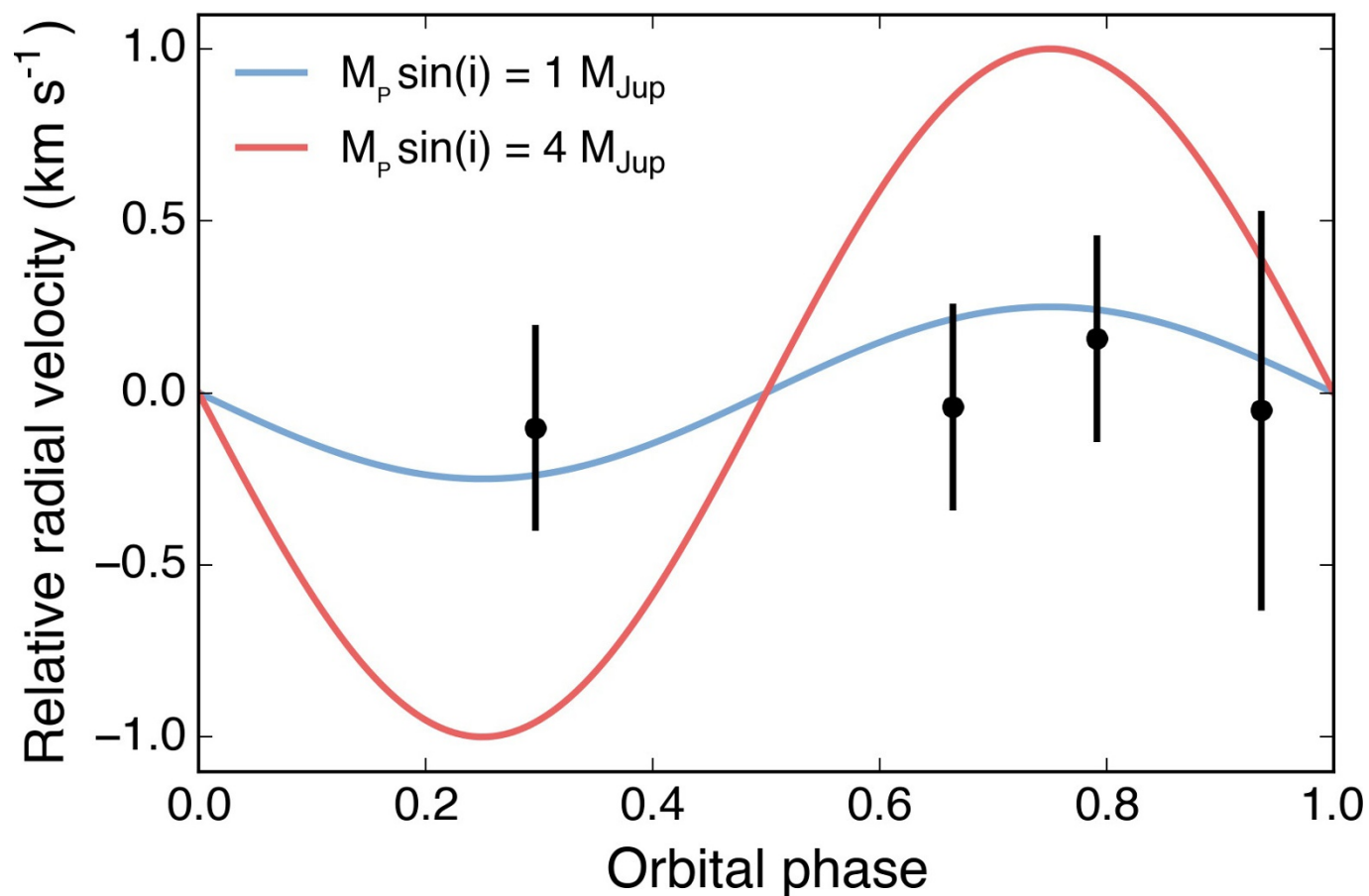
Extended Data Figure 1 | K2 light curve for K2-33 phased on the stellar rotation period of 6.3 days. Semi-sinusoidal brightness variations due to rotational modulation of starspots. Point colour indicates the relative time of observation, with grey corresponding to earlier in the campaign and dark blue corresponding to later times. Brightness is lowest when the most heavily spotted hemisphere of the stellar surface is along the line of sight.

The shape and evolution of the variability pattern depends on the number, geometry, distribution, and lifetime of spots, along with any latitudinal gradient in the rotational speed (differential rotation). The transits of K2-33 b are visible by eye in this figure and are too narrow in rotational phase to be attributed to any feature on or near the stellar surface.



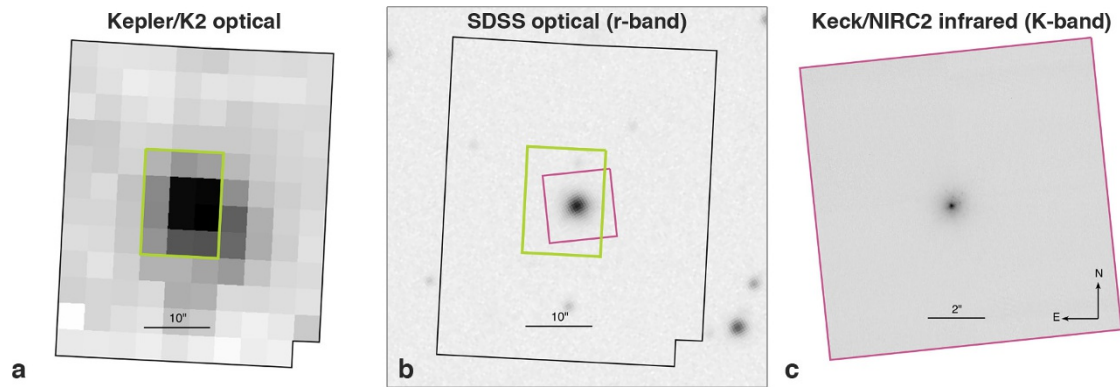
Extended Data Figure 2 | Model-dependent age of K2-33. **a**, Solid lines show mean stellar density as a function of effective temperature for pre-main-sequence stars having different ages, according to theoretical models¹⁹. Grey points represent plausible combinations of density and temperature for K2-33 as determined by light-curve fits and stellar

spectroscopy. **b**, Distribution of implied stellar age based on temperature, density, and pre-main-sequence models. The implied age of 2–7 Myr is consistent with the age we adopted of 5–10 Myr, derived independently. Dark- and light-grey shaded regions indicate 68% and 95% confidence intervals, respectively.



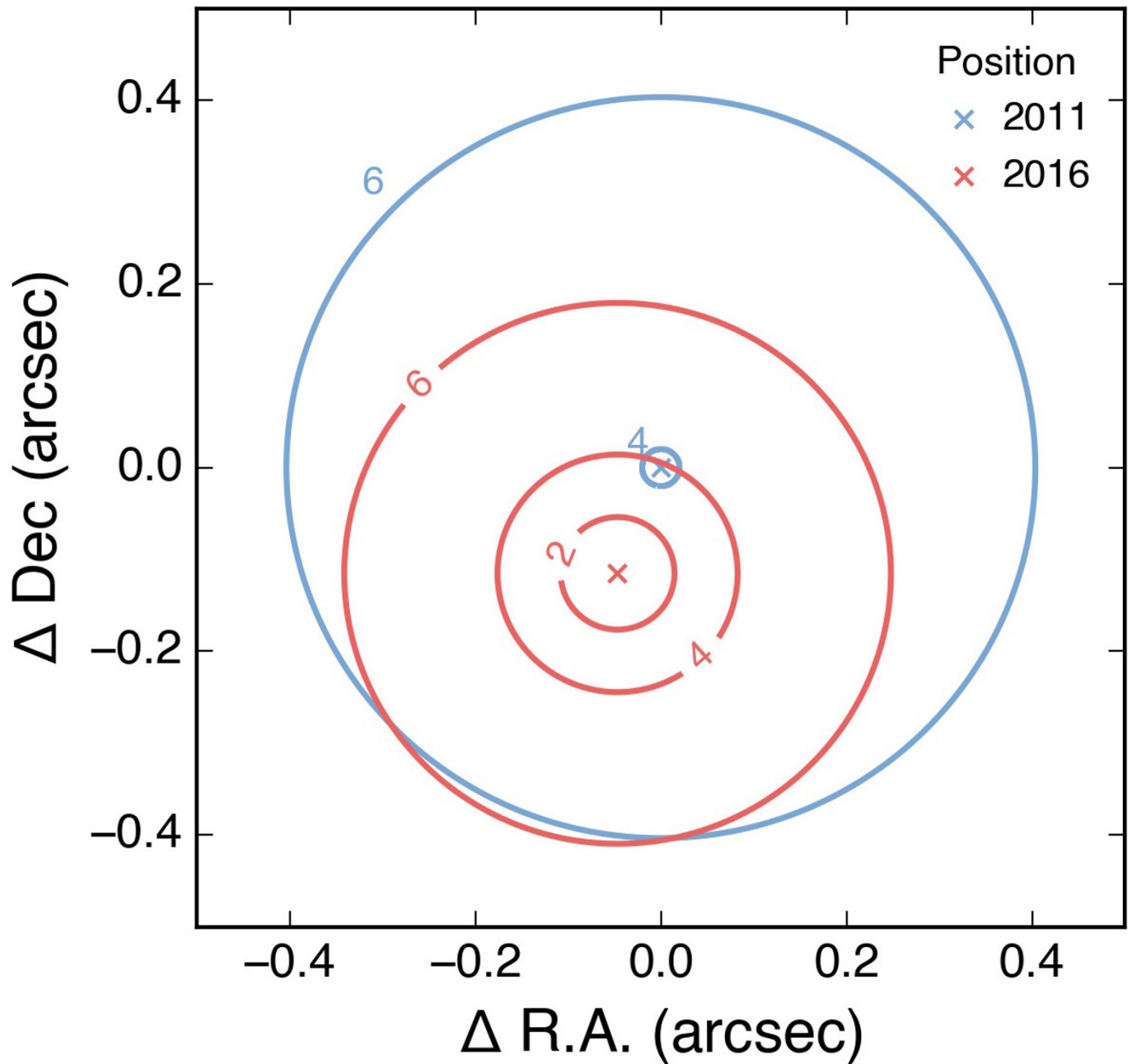
Extended Data Figure 3 | Apparent radial velocity variations of K2-33. Line-of-sight velocities and 1σ uncertainties (standard deviations, indicated by error bars) with respect to the Solar System barycentre from Keck/HIRES are indicated. Radial velocities are mean-subtracted, and the abscissa shows the orbital phase of K2-33 b measured from K2 photometry (mid-transit occurs at zero orbital phase). We rule out radial velocity

variations larger than 300 m s^{-1} at 68.3% confidence, corresponding to a $1.2M_{\text{Jup}}$ planet mass. Curves show the expected radial velocity variations for planets having circular orbits and different masses M_p . Radial velocities due to a $1.0M_{\text{Jup}}$ planet (blue) are consistent with our observations, while a $4.0M_{\text{Jup}}$ planet (red) is ruled out at high confidence.



Extended Data Figure 4 | Images of K2-33. **a**, K2 target pixel file. **b**, Sloan Digital Sky Survey (SDSS) optical image. **c**, Keck/NIRC2 K-band image. Extents of the K2 target pixel file, K2 photometric aperture, and NIRC2 image are shown respectively with black, green, and purple boundaries. In each image, north is up and east is left. Three other sources identified by

SDSS reside within the K2 photometric aperture, one of which is a galaxy. All are 7.3–10.1 magnitudes fainter than K2-33 in the SDSS r-filter and below the detection limit of the NIRC2 images, and are thus too faint to produce the observed transits.



Extended Data Figure 5 | Sensitivity to non-comoving sources in the vicinity of K2-33. The blue X marks the star's position in 2011. Between 2011 and 2016, the star moved by $0.1228'' \pm 0.0085''$ (red X) owing to proper motion. Contours show the K-band sensitivity to non-comoving stars from adaptive optics imaging from both epochs. The 2011 data

set included non-redundant aperture masking, and provided tighter constraints. The combined sensitivity to non-comoving objects is the maximum contrast achieved for either data set. Owing to stellar proper motion, we achieved K-band contrasts of >3.3 mag throughout the $\Delta\text{RA}-\Delta\text{dec.}$ plane, even at the 2011 and 2016 positions of K2-33.

Extended Data Table 1 | Keck/HIRES radial velocities for K2-33

Epoch (UTC)	BJD	Radial velocity (km s ⁻¹)
2015-06-01 12:57:36.0	2457175.040	-6.61 ± 0.58
2016-02-02 15:30:14.4	2457421.146	-6.66 ± 0.30
2016-02-04 15:23:02.4	2457423.141	-6.60 ± 0.30
2016-02-21 14:29:45.6	2457440.104	-6.40 ± 0.30

Line-of-sight velocities and 1σ uncertainties (standard deviations) with respect to the Solar System barycentre. UTC, Coordinated Universal time.